

Stabilizing Decentralized Federated Fine-Tuning via Topology-Aware Alternating LoRA

Xiaoyu Wang, Xiaotian Li, Zhixiang Zhou, Chen Li, and Yong Liu

Department of Electrical and Computer Engineering, New York University, Brooklyn, NY, USA

Email: wang.xiaoyu@nyu.edu, xl3399@nyu.edu, zz4819@nyu.edu, chen.lee@nyu.edu, yongliu@nyu.edu

Abstract—Decentralized federated learning (DFL), a serverless variant of federated learning, poses unique challenges for parameter-efficient fine-tuning due to the factorized structure of low-rank adaptation (LoRA). Unlike linear parameters, decentralized aggregation of LoRA updates introduces topology-dependent cross terms that can destabilize training under dynamic communication graphs. We propose **TAD-LoRA**, a Topology-Aware Decentralized Low-Rank Adaptation framework that coordinates the updates and mixing of LoRA factors to control inter-client misalignment. We theoretically prove the convergence of **TAD-LoRA** under non-convex objectives, explicitly characterizing the trade-off between topology-induced cross-term error and block-coordinate representation bias governed by the switching interval of alternative training. Experiments under various communication conditions validate our analysis, showing that **TAD-LoRA** achieves robust performance across different communication scenarios, remaining competitive in strongly connected topologies and delivering clear gains under moderately and weakly connected topologies, with particularly strong results on the MNLI dataset.

Index Terms—Federated learning, Decentralized Federated Learning, Low-rank Adaptation, Alternating Optimization, Parameter-efficient Fine-tuning.

I. INTRODUCTION

Large Language Models (LLMs) such as GPT [1], LLaMA [2], GLM [3], and DeepSeek [4] have achieved state-of-the-art performance on diverse language tasks. Adapting these models in a privacy-preserving manner motivates federated learning (FL), where data remain distributed across clients. Parameter-efficient fine-tuning (PEFT) methods, especially LoRA [5], are attractive for FL due to their small memory and communication footprints. LoRA introduces trainable low-rank factors A and B , but aggregating these matrices directly in FL creates a bilinear inconsistency: averaging A and B independently produces cross-client interactions $B_i A_j$ ($i \neq j$) that distort the global update and degrade convergence.

Several recent studies have attempted to mitigate this challenge. FLoRA [6] eliminates cross terms via block-diagonal stacking, at the cost of parameter growth proportional to the number of clients. FlexLoRA [7] reconstructs unified updates using SVD, but suffers from scalability issues due to costly server-side factorization. FFA-LoRA [8] fixes one LoRA matrix across all clients to prevent bilinear interference, though sacrificing the model expressiveness.

A recent line of work shows that *alternating* the optimization of A and B stabilizes LoRA aggregation in *centralized* FL (CFL) by ensuring that only one block is updated and

aggregated per round [9]. However, this mechanism relies on strict synchronization: all clients must periodically synchronize parameters with the server and follow an identical alternative training schedule. In decentralized FL (DFL), where clients mix parameters only with their neighbors, information propagates gradually and client states drift within each phase [10]. As a result, the key assumptions enabling cross-term suppression in centralized alternating LoRA no longer hold in DFL setting.

This paper revisits alternating LoRA through the lens of DFL and asks: *how can alternating low-rank updates be made stable and effective with asynchronous peer-to-peer model aggregation?*

We show that decentralized mixing interacts with block-coordinate updates in a nontrivial way, leading to phase-state mismatch and drift between LoRA directions. To address these issues, we introduce **TAD-LoRA**, a topology-aware decentralized alternating LoRA framework that incorporates (i) interval-based directional switching, and (ii) joint mixing of both LoRA blocks to maintain cross-client alignment. This yields a more stable alternating process and keeps decentralized LoRA training effective even on challenging NLP tasks.

Our main contributions are summarized as follows:

- We identify a fundamental instability of alternating LoRA in *decentralized federated learning*, showing that asynchronous peer-to-peer mixing of factorized updates introduces a topology-dependent cross term and block-wise state mismatch that are absent in *centralized federated learning*.
- We propose **TAD-LoRA**, a topology-aware decentralized alternating scheme that updates a single low-rank block at a time while jointly mixing both LoRA factors, enabling more consistent parameter states across clients under dynamic communication graphs.
- We provide the first convergence analysis of decentralized alternating LoRA, explicitly characterizing the trade-off between topology-induced cross-term error, which decreases with the switching interval T , and centralized block-coordinate representation bias, which increases with T . Under a local PL condition, we derive a topology-dependent optimal switching interval T^* that depends on the underlying communication reliability and network connectivity.
- Through extensive experiments across, we demonstrate

that TAD-LoRA achieves consistent and robust performance across a wide range of communication scenarios: it remains competitive in strongly connected networks while providing clear gains under moderately and weakly connected networks, outperforming decentralized baselines on final accuracy, with particularly strong results on MNLI.

II. RELATED WORK

A. Federated Learning

Federated learning (FL) enables collaborative training across distributed clients without sharing raw data [11]. Key challenges include data heterogeneity [12], partial client participation [13], and high communication cost [14]. To reduce communication overhead, prior work explores model compression [15], sparse updates [16], personalized models [17], and adaptive aggregation schemes. Decentralized FL [10], [18], [19] and asynchronous FL [20] offload or eliminate the central server, making client states evolve at different rates and complicating convergence analysis. Our work examines these issues specifically for LoRA-based low-rank adaptation, where the bilinear parameterization introduces unique aggregation inconsistencies under both CFL and DFL.

B. LoRA in Federated Learning

LoRA [5] is widely adopted in FL due to its low communication cost and parameter efficiency. Several variants extend LoRA to heterogeneous and personalized settings, including SLoRA [21], FedSA-LoRA [22], and pFedLoRA [23]. These methods address client diversity but do not resolve the bilinear inconsistency inherent to aggregating independently trained LoRA factors. A complementary line of work tackles this issue directly. FLoRA [6] uses block-diagonal concatenation to avoid cross terms but enlarges model size; FlexLoRA [7] reconstructs global updates via SVD; and FFA-LoRA [8] freezes one LoRA matrix to suppress cross-client interference. While effective, these methods trade off scalability, flexibility, or representational capacity.

Most relevant to this work, RoLoRA [9] shows that alternating updates of A and B improve stability in *centralized* FL. However, its analysis assumes synchronous rounds and server-enforced parameter consistency, and evaluates only fixed odd-even schedules under centralized aggregation. Whether alternating LoRA remains stable in decentralized peer-to-peer settings—where clients mix stale parameters and cannot maintain a shared frozen block—has not been investigated, and naive extensions behave poorly in practice.

Beyond federated settings, AltLoRA [24] applies alternating projections to improve gradient approximation in centralized single-machine fine-tuning. This literature focuses on optimization quality rather than multi-client aggregation and is orthogonal to our study of alternating LoRA under communication-constrained FL.

III. MOTIVATION AND ANALYSIS

LoRA models a weight update using a low-rank factorization $\Delta W = BA$. In federated learning, each client updates local *factors* (A_i, B_i) , and aggregation is performed on each factor rather than their product:

$$A^{\text{agg}} = \sum_i w_i A_i, \quad B^{\text{agg}} = \sum_i w_i B_i,$$

and reconstructing the update gives

$$B^{\text{agg}} A^{\text{agg}} = \underbrace{\sum_i w_i^2 B_i A_i}_{\text{desired average update}} + \underbrace{\sum_{i \neq j} w_i w_j B_i A_j}_{\text{cross-client interference}}.$$

The first term corresponds to the desired average update, while the second mixes B_i from one client with A_j from another—an update direction that no client ever computed. These cross terms are a primary source of instability when LoRA is trained on heterogeneous data.

a) Why alternating works in centralized FL.: In centralized federated learning (CFL), alternating updates eliminate these cross terms [9]. During a B-phase, all clients share the same A , so $B_i A$ averages cleanly; during an A-phase, they share the same B , so $B A_i$ averages cleanly. Server-enforced synchronization ensures that the frozen block is identical across clients, restoring the stability of two-block coordinate descent.

b) Challenges of Alternating LoRA in Decentralized Settings.: In decentralized federated learning (DFL), this synchronization assumption no longer holds. Clients exchange parameters only with neighbors, so even within the same logical phase, their local models may differ due to incomplete information propagation. As a result, the frozen block is no longer shared across clients, and alternating updates can no longer fully suppress cross terms. This leads to two DFL-specific effects:

- **Phase-state mismatch:** clients enter the same phase with different versions of the frozen block.
- **Block-wise drift:** discrepancies in the frozen block accumulate over time, reintroducing cross-client interactions during mixing.

The issue can be illustrated by the following example:

client i holds A_i and receives $A_j \neq A_i$ from neighbors
 \Rightarrow the B-phase can no longer eliminate $B_i A_j$ cross terms.

These effects induce a fundamental trade-off. Methods such as RoLoRA, which alternate frequently without coordinating frozen-block mixing, suffer from block misalignment under sparse communication. In contrast, FFA-LoRA, which uses very infrequent switching, mitigates misalignment but amplifies cross-term noise due to prolonged staleness. This trade-off suggests that the switching interval must be jointly considered with communication conditions, motivating the topology-aware coordination mechanism in TAD-LoRA.

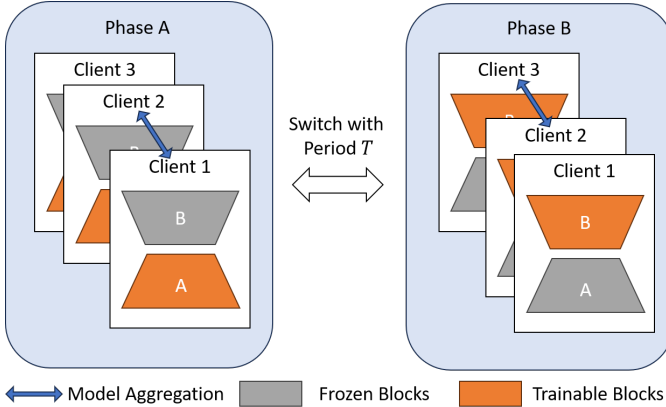


Fig. 1: Overall illustration of TAD-LoRA under decentralized federated learning (DFL). Clients communicate directly with a dynamically selected subset of peers in a peer-to-peer manner, as determined by the underlying communication topology. At each alternating phase (lasting T rounds), A-blocks or B-blocks are actively updated and coordinated across clients, while the other remains frozen during that phase and is aligned implicitly through topology-aware switching over time.

IV. METHODOLOGY

The above analysis shows that decentralized communication disrupts the synchronization required for alternating LoRA to remain stable, mainly due to phase-state mismatch and block-wise drift resulted from asynchronous P2P model mixing. To study and mitigate these effects, we first formalize the decentralized FL communication model, and then introduce our joint-mixing alternating LoRA procedure. Overview of the TAD-LoRA framework is at Fig 1

A. Decentralized FL Communication Model

We adopt a standard decentralized FL (DFL) setting where clients maintain local parameters and exchange them with neighbors through a time-varying mixing matrix W_t :

$$x_i^{t+1} = \sum_{j=1}^N (W_t)_{ij} x_j^t.$$

The matrices $\{W_t\}$ are *doubly-stochastic* and satisfy standard connectivity and spectral-gap assumptions used in decentralized optimization. All clients perform local updates every round. Communication is serverless: each round consists of (i) local computation and (ii) optional peer-to-peer mixing when communication is triggered. This contrasts with centralized FL (CFL), where a parameter server enforces identical global states at each round.

B. Alternating LoRA in FL

LoRA represents a low-rank update as $\Delta W = BA$, where A and B denote the down- and up-projection matrices. Alternating LoRA updates only one block per phase:

$$A_i^{t+1} = A_i^t - \eta \nabla_A \mathcal{L}_i(A_i^t, B_i^t), \quad B_i^{t+1} = B_i^t,$$

during the A-phase, and symmetrically for the B-phase. This block splitting removes LoRA cross terms and stabilizes optimization.

CFL: Centralized Alternating LoRA (RoLoRA). In centralized FL, all clients follow identical A/B phases and the server conducts model aggregation through FedAvg:

$$A^{t+1} = \frac{1}{N} \sum_{i=1}^m A_i^{t+1}, \quad B^{t+1} = \frac{1}{N} \sum_{i=1}^m B_i^{t+1}.$$

Since only the active block is aggregated in each phase, the centralized procedure behaves as standard two-block coordinate descent.

DFL: Decentralized Alternating LoRA Baseline. In DFL, aggregation is replaced by peer-to-peer mixing, but only the *active* block is synchronized. During an A-phase:

$$A_i^{t+1} = \sum_j (W_t)_{ij} A_j^t, \quad B_i^{t+1} = B_i^t,$$

and during a B-phase:

$$B_i^{t+1} = \sum_j (W_t)_{ij} B_j^t, \quad A_i^{t+1} = A_i^t.$$

Because the frozen block is not synchronized across clients during its inactive phase, clients gradually accumulate inconsistent versions of it, leading to *phase-state mismatch* and block-wise drift, the main failure mode of alternating LoRA under DFL.

C. TAD-LoRA: Joint-Mixing Alternating LoRA

To mitigate drift in decentralized alternating LoRA, we introduce TAD-LoRA, which synchronizes both LoRA blocks in every round, regardless of which block is being updated. After local updates, each client performs joint mixing:

$$A_i^{t+1} = \sum_j (W_t)_{ij} A_j^t, \quad B_i^{t+1} = \sum_j (W_t)_{ij} B_j^t.$$

Joint mixing reduces the frozen block misalignment across the network, mitigating phase-state mismatch and stabilizing alternating LoRA under decentralized communication.

We study a decentralized learning process over R communication rounds, where each round $t \in \{0, \dots, R-1\}$ consists of a local update followed by a communication-induced mixing step.

Algorithm 1 summarizes the full procedure.

Throughout the paper, we use the terms *iteration* and *round* interchangeably to denote one local update followed by a communication-induced mixing step.

V. CONVERGENCE ANALYSIS & SWITCHING INTERVAL

We present a convergence analysis of decentralized alternating LoRA under time-varying topologies, focusing on the trade-off governed by the switching interval T . We demonstrate that while a larger T enhances inter-client consensus by suppressing topology-induced errors, it inevitably introduces a *centralized representation bias* due to stale updates. To quantify this balance, we decompose the averaged LoRA

Algorithm 1 TAD-LoRA: Joint-Mixing Alternating LoRA in Decentralized FL

Require: Initial blocks $\{(A_i^0, B_i^0)\}_{i=1}^m$; total rounds R ; switching interval T ; mixing matrices $\{W_t\}_{t=0}^{R-1}$.

- 1: **for** $t = 0, \dots, R-1$ **do**
- 2: **if** $\lfloor t/T \rfloor$ is even **then**
- 3: **B-phase:** each client i updates B_i^t locally while keeping A_i^t fixed.
- 4: **else**
- 5: **A-phase:** each client i updates A_i^t locally while keeping B_i^t fixed.
- 6: **end if**
- 7: **Joint mixing:** for each client i ,
- 8: $A_i^{t+1} \leftarrow \sum_{j=1}^m (W_t)_{ij} A_j^t$
- 9: $B_i^{t+1} \leftarrow \sum_{j=1}^m (W_t)_{ij} B_j^t$
- 10: **end for**

update and establish a stationarity bound under dynamic connectivity. Finally, assuming a local PL condition, we derive the convergence rate and characterize the topology-dependent optimal switching interval $T^*(\rho)$.

A. Setup and Assumptions

We consider the LoRA parameterization $\theta = \theta_0 + BA$, where client i holds local blocks (A_i^t, B_i^t) to optimize the global objective $F(\theta) = \frac{1}{m} \sum_{i=1}^m f_i(\theta)$. Communication is governed by time-varying, doubly-stochastic mixing matrices W_t satisfying the mean-square contraction property $\mathbb{E}\|W_t - \frac{1}{m}\mathbf{1}\mathbf{1}^\top\|_2^2 \leq \rho^2$ with $\rho \in (0, 1)$.

For analysis, we define the averaged blocks \bar{A}^t, \bar{B}^t and the averaged model $\bar{\theta}^t$. Consensus is measured by the block disagreements $\|\Delta_A^t\|^2 := \frac{1}{m} \sum_i \|A_i^t - \bar{A}^t\|_F^2$ and $\|\Delta_B^t\|^2 := \frac{1}{m} \sum_i \|B_i^t - \bar{B}^t\|_F^2$.

In addition to standard regularity conditions (e.g., L -smoothness, bounded stochastic gradients) detailed in Appendix A-B, our analysis relies on two structural assumptions specific to the alternating LoRA landscape. To streamline notation, we define the following reference values:

- Let θ_1^* be the optimal parameter of the centralized alternating LoRA with $T = 1$.
- Let $F_1^* := F(\theta_1^*)$ denote the corresponding optimal function value.
- Let F_T^* denote the optimal function value achievable with a switching interval T .

Assumption V.1 (Local Polyak–Łojasiewicz (PL) condition on the LoRA subspace). There exists a constant $\mu > 0$ such that for all θ in a neighborhood of θ_1^* , the suboptimality relative to the $T = 1$ baseline is bounded by the gradient:

$$F(\theta) - F_1^* \leq \frac{1}{2\mu} \|\nabla F(\theta)\|^2.$$

While the PL condition governs the convergence rate, coarse-grained alternation ($T > 1$) introduces a structural bias by restricting the optimization trajectory. We quantify this cost relative to the reference $T = 1$ baseline as follows.

Assumption V.2 (Alternating-induced factorization bias). There exists a constant $C_3 > 0$ such that, for a sufficiently small stepsize η , the gap between the T -interval optimum and the $T = 1$ baseline satisfies:

$$\phi(T) := F_T^* - F_1^* \leq C_3 \eta^2 T.$$

B. Error Decomposition and Consensus Mechanism

Unlike linear models, the distributed averaging of LoRA parameters introduces a non-linear discrepancy. To analyze this, we decompose the global update matrix $\bar{W}^t := \frac{1}{m} \sum_i B_i^t A_i^t$ into a centralized-equivalent term and a topology-dependent error:

$$\bar{W}^t = \bar{B}^t \bar{A}^t + C^t, \quad \text{where } \|C^t\|_F \leq \|\Delta_A^t\| \|\Delta_B^t\|.$$

This inequality (derived via Cauchy–Schwarz) reveals that the deviation from the centralized trajectory is controlled strictly by the consensus error. This motivates our analysis of how the switching interval T affects block disagreement.

Under standard assumptions (smoothness, bounded gradients, and mixing contraction ρ), we establish that frozen blocks contract purely via gossip, while updated blocks reach a steady-state error (Lemma A.4 in Appendix). Consequently, increasing the switching interval allows the frozen block to benefit from $T - 1$ additional gossip steps. We quantify this effect by bounding the cycle-averaged cross term (see Appendix A-E):

$$\frac{1}{T} \sum_{\tau=0}^{T-1} \mathbb{E}\|C^{t+\tau}\|_F \leq \frac{C_{\text{cr}} \eta^2}{T(1-\rho)}.$$

This result is pivotal: it demonstrates that extending the alternating period T explicitly suppresses the topology-induced error by a factor of $1/T$, effectively "buying" consensus with time.

C. Convergence and Topology-Dependent Trade-off

Building on the cross-term bound, we derive the global convergence guarantees. We first establish a stationarity bound for the averaged model $\bar{\theta}^t$, which allows us to translate the gradient norm into function-value suboptimality. By incorporating the Local PL condition (Assumption V.1) and the alternating-induced bias $\phi(T)$ (Assumption V.2), we obtain our main convergence result relative to the centralized baseline F_1^* :

Theorem V.3 (Convergence Rate and Trade-off). *Let $\hat{\theta}_R$ be sampled uniformly from the trajectory. The suboptimality is bounded by:*

$$\begin{aligned} \mathbb{E}[F(\hat{\theta}_R) - F_1^*] &\leq \underbrace{\frac{1}{2\mu} \left(\frac{C_0}{\eta R} + C_1 \eta \right)}_{\text{Optimization Error}} \\ &\quad + \underbrace{\frac{C_2 \eta^2}{2\mu T(1-\rho)}}_{\text{Topology Error}} + \underbrace{\phi(T)}_{\text{Bias}}. \end{aligned} \tag{V.1}$$

Theorem V.3 formalizes the fundamental tension in our method. Neglecting vanishing optimization terms, the performance is governed by $\Psi(T) := \frac{C_2 \eta^2}{2\mu T(1-\rho)} + \phi(T)$. The

topology error decreases with T , while the representation bias $\phi(T)$ (bounded by $O(T\eta^2)$) increases with T . Minimizing $\Psi(T)$ yields the topology-dependent optimal interval:

$$T^*(\rho) \simeq \Theta\left(\frac{1}{\sqrt{1-\rho}}\right).$$

This implies that in poorly connected networks (large ρ), a larger switching interval T is necessary to suppress communication errors, whereas well-connected networks favor smaller T to mitigate representation bias.

Discussion. In practice, due to discrete scheduling and training noise, this tradeoff often manifests as a range of effective switching intervals rather than a single sharp optimum. Our analysis establishes a non-monotonic dependence of performance on the switching interval, implying the existence of an optimal regime rather than a universally best fixed choice. We will empirically examine this behavior in the following section.

VI. EXPERIMENTS

A. Experimental Setup

We evaluate TAD-LoRA on four representative GLUE tasks (SST-2, QNLI, QQP, MNLI). Unless otherwise specified, we follow the experimental setup of [8] for all tasks, models, and training configurations.

1) *Model Configuration.*: We use **RoBERTa-Large** (335M) with LoRA applied to the **Q/V** projections ($r = 8$, $\alpha = 16$, dropout 0.1). The classification head is frozen.

2) *Federated Learning Settings.*:

Data Partitions.: For binary tasks, 10 clients follow $3 \times [0.9, 0.1]$, $3 \times [0.1, 0.9]$, $4 \times [0.5, 0.5]$; for MNLI, $4 \times [0.9, 0.05, 0.05]$, $3 \times [0.05, 0.9, 0.05]$, $3 \times [0.05, 0.05, 0.9]$.

Communication Topology.: Different from [8], we consider a decentralized federated learning (DFL) setting with explicit network topologies. We adopt a commonly used random communication topology, corresponding to an Erdős-Rényi graph [25] with edge activation probability p , for decentralized training. At each round, each client exchanges model updates with peers independently with probability p , capturing typical information mixing behavior. We vary $p \in \{0.5, 0.2, 0.1, 0.05, 0.02, 0.01\}$, covering regimes from dense to extremely sparse communication. Due to space constraints, the main results focus on this representative topology, while results under more structured topologies (e.g., ring networks) are reported in the appendix.

Choice of switching intervals.: We fix the total training horizon to $R = 150$ rounds. To avoid asymmetric updates caused by an incomplete final alternation cycle, we only consider switching intervals T that evenly divide R . In preliminary experiments, we observed higher run-to-run variance when $T \nmid R$ (e.g., $T = 7$ or $T = 20$). We therefore restrict T to divisors of R (e.g., $T \in \{1, 2, 3, 5, 10, 15\}$) for stable and reproducible estimation of $\hat{T}^*(p)$.

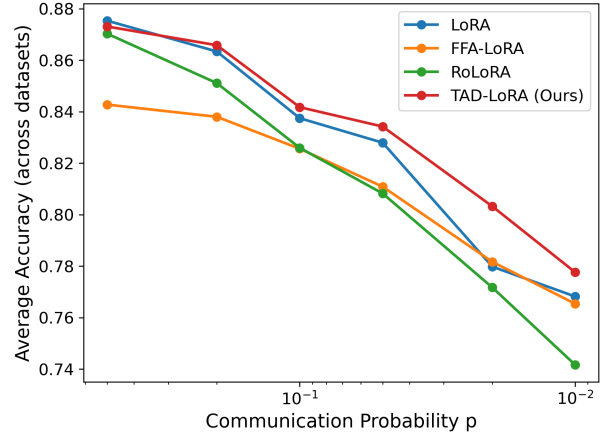


Fig. 2: Average test accuracy across datasets under different communication probabilities p . LoRA denotes the vanilla decentralized LoRA baseline with FedAvg [11]; FFA-LoRA fixes one LoRA factor during training; RoLoRA alternates LoRA factors in a naive round-robin manner; TAD-LoRA is our topology-aware decentralized alternating LoRA. As communication becomes weaker (smaller p), TAD-LoRA consistently outperforms all baselines, while remaining competitive under strong communication.

3) *Baselines.*: We compare TAD-LoRA with following baselines:

- LoRA: Standard LoRA fine-tuning under decentralized federated learning, where both LoRA matrices are locally trained and aggregated via FedAvg.
- FFA-LoRA [8]: A LoRA variant that freezes A and only updates B , effectively restricting adaptation to a fixed low-dimensional subspace.
- RoLoRA [9]: A centralized alternating LoRA method extended to DFL by aggregating only the active trainable parameters. Following the original paper, we use a per-round alternation, i.e., $T = 1$.
- TAD-LoRA: our topology-aware joint-mixing decentralized alternating LoRA method.

4) *Training and Evaluation Details.*: Each FL round uses **20 local steps**, for **150 rounds** total. We use AdamW (HuggingFace defaults), sequence length 128, batch size 32, and search learning rate over $\{2 \times 10^{-4}, 5 \times 10^{-4}, 1 \times 10^{-3}, 2 \times 10^{-3}, 5 \times 10^{-3}\}$. All experiments run on NVIDIA RTX8000 clusters. In DFL, no global model exists. For each seed, we evaluate all 10 client models and compute the **mean accuracy across clients**. We then report the **mean and standard deviation across random seeds** as the final performance.

B. Main Results

Overall performance under varying communication probabilities. Figure 2 shows the average test accuracy across datasets under different communication probabilities p . While all methods (except FFA-LoRA) perform similarly under strong communication, clear performance gaps emerge as

communication becomes sparser. In particular, TAD-LoRA exhibits increasingly larger gains as p decreases, consistently outperforming prior methods in both moderate and weak communication regimes. These results indicate that naive alternating strategies fail to properly handle staleness and block misalignment under limited communication, whereas topology-aware alternating becomes increasingly important as communication constraints intensify. We also observe complementary trends between RoLoRA and FFA-LoRA, which provide additional evidence for our analysis. RoLoRA can be viewed as an alternating baseline without coordinating the mixing of the frozen block, whereas FFA-LoRA corresponds to an extreme case with very infrequent switching (i.e., large T). Consistent with the proposed trade-off, RoLoRA tends to perform well when communication is strong but degrades rapidly as p decreases, suggesting that insufficient frozen-block mixing leads to pronounced misalignment under sparse communication. In contrast, FFA-LoRA becomes relatively more competitive in low- p regimes, aligning with the intuition that less frequent alternation can mitigate cross-term effects when synchronization is severely limited. Overall, these contrasting behaviors corroborate the need to jointly coordinate switching and block mixing, which is exactly what TAD-LoRA achieves. Both baselines are limited by incomplete *client-level coordination* of the active LoRA block across alternating phases, which becomes increasingly harmful as communication becomes sparse.

Quantitative comparison under representative regimes. Table I reports detailed results under representative strong ($p = 0.5$), moderate ($p = 0.1$), and weak ($p = 0.02$) communication regimes. Under strong communication ($p = 0.5$), TAD-LoRA achieves comparable performance to the strongest baselines. Under moderate communication ($p = 0.1$), TAD-LoRA already achieves the best or near-best performance across individual datasets, demonstrating that the benefits of topology-aware alternating emerge well before entering extreme communication sparsity. Under weak communication ($p = 0.02$), TAD-LoRA consistently attains the strongest performance across nearly all datasets, rather than being driven by improvements on a single task. Together, these results highlight the per-dataset robustness of TAD-LoRA and its effectiveness across a wide spectrum of communication conditions.

C. Ablation Study

Topology-aware selection of the switching interval. Our theoretical analysis suggests that the optimal switching interval should adapt to the underlying network connectivity. For Erdős-Rényi graphs with edge activation probability p , the effective connectivity improves monotonically with p , leading to different preferred switching regimes across communication conditions.

Motivated by this insight, we evaluate TAD-LoRA under different values of p and sweep the switching interval T accordingly. We observe that sparser graphs (smaller p) tend to favor larger switching intervals, while denser graphs achieve

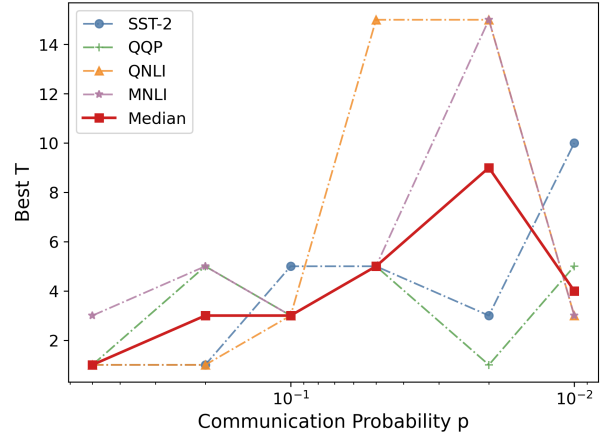


Fig. 3: Dataset-wise optimal switching interval $\hat{T}^*(p)$ (thin dashed lines) and the **Median** trend across datasets (thick line). The median aggregation mitigates the high variance introduced by argmax-based selection over a discrete candidate set. In the reliably convergent regime $p \geq 0.02$, the **Median** trend shifts toward larger T as communication becomes weaker, consistent with the monotonicity predicted by our theory.

their best performance with more frequent alternation. This behavior is consistent with the non-monotonic dependence on T predicted by the theory (see Appendix A-J).

Aggregate trend of the optimal switching interval While the theory characterizes a population-level trend, we empirically estimate $\hat{T}^*(p)$ for analysis purposes by selecting the best interval from a *discrete candidate set* considered in the experimental setup, via a *noisy argmax* over performance averaged across multiple random seeds and a finite training horizon. As a result, $\hat{T}^*(p)$ is sensitive to discretization effects and run-to-run variance, which may introduce local deviations from the overall trend.

To mitigate such noise, Figure 3 reports the *median optimal switching interval across datasets*. Focusing on the reliably convergent regime $p \geq 0.02$, the median trend shifts toward larger T as communication becomes weaker, supporting the monotonic trend predicted by our theory at the aggregate level. At extremely sparse communication (e.g., $p = 0.01$), the estimate becomes higher-variance and may deviate from the trend, which is consistent with the instability of argmax-based selection. Dataset-wise optimal intervals and aggregate statistics are reported in Appendix IV.

From aggregate trends to instance-level behavior. The median optimal switching interval in Figure 3 reveals a clear population-level trend: as communication becomes weaker (p decreases), the optimal switching interval shifts toward larger values. To further understand this behavior at a finer granularity, Figure 4 shows the accuracy gain of TAD-LoRA over the LoRA baseline on MNLI across different communication probabilities p and switching intervals T . Under weak communication (small p), performance gains concentrate on moderate to larger T and span a wider range of effective

TABLE I: Test accuracy (mean \pm variance) under representative strong ($p = 0.5$), moderate ($p = 0.1$), and extremely weak ($p = 0.02$) communication regimes. For each p , best and second-best results are highlighted.

p	Method	SST-2	QQP	QNLI	MNLI	Avg.
0.5	LoRA	0.9468 \pm 0.0019	0.8347 \pm 0.0085	0.9067 \pm 0.0043	<u>0.8132</u> \pm 0.0194	0.8754
	FFA-LoRA	0.9436 \pm 0.0032	0.8051 \pm 0.0061	0.8911 \pm 0.0036	0.7313 \pm 0.0333	0.8428
	RoLoRA	<u>0.9462</u> \pm 0.0023	0.8216 \pm 0.0108	<u>0.9021</u> \pm 0.0031	0.8115 \pm 0.0088	0.8703
	TAD-LoRA (Ours)	0.9448 \pm 0.0007	<u>0.8328</u> \pm 0.0072	0.9003 \pm 0.0048	0.8145 \pm 0.0066	<u>0.8731</u>
0.1	LoRA	0.9370 \pm 0.0058	0.8098 \pm 0.0076	0.8779 \pm 0.0159	0.7253 \pm 0.0440	0.8375
	FFA-LoRA	0.9313 \pm 0.0046	0.7915 \pm 0.0086	0.8710 \pm 0.0048	0.7086 \pm 0.0242	0.8256
	RoLoRA	0.9325 \pm 0.0048	0.7890 \pm 0.0027	0.8711 \pm 0.0045	0.7113 \pm 0.0133	0.8260
	TAD-LoRA (Ours)	0.9401 \pm 0.0019	<u>0.8050</u> \pm 0.0073	0.8815 \pm 0.0145	0.7405 \pm 0.0376	0.8418
0.02	LoRA	0.8668 \pm 0.0811	<u>0.7702</u> \pm 0.0066	0.8416 \pm 0.0031	0.6407 \pm 0.0118	0.7798
	FFA-LoRA	<u>0.9186</u> \pm 0.0038	0.7627 \pm 0.0121	0.8264 \pm 0.0178	0.6191 \pm 0.0358	<u>0.7817</u>
	RoLoRA	0.9147 \pm 0.0022	0.7582 \pm 0.0116	0.8160 \pm 0.0045	0.5980 \pm 0.0291	0.7717
	TAD-LoRA (Ours)	0.9263 \pm 0.0019	0.7783 \pm 0.0036	0.8480 \pm 0.0063	0.6604 \pm 0.0408	0.8032

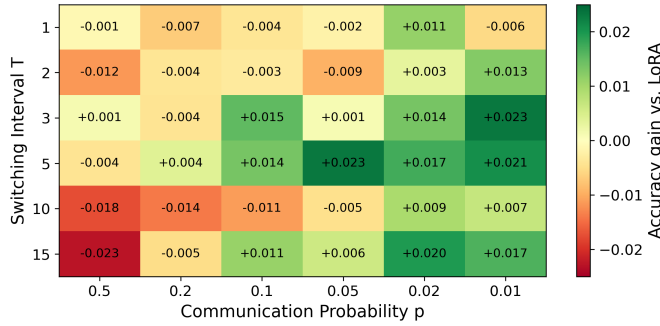


Fig. 4: Accuracy gain of TAD-LoRA over the LoRA baseline on MNLI under different communication probabilities p and switching intervals T . Positive values indicate performance improvement over LoRA. Under weak communication (small p), performance gains concentrate on moderate to larger T and span a wider range of effective switching intervals.

switching intervals. As communication becomes stronger, the sensitivity to T diminishes, indicating improved robustness to the choice of the switching interval.

Additional result are deferred to the appendix.

D. Switching Interval Selection in Practice

In our experiments, the best switching intervals are selected in hindsight to characterize the performance landscape and isolate the effect of T . Importantly, our results show that under weak communication, a broad range of switching intervals yields consistent improvements, indicating robustness to imperfect T selection. A simple practical heuristic is to use smaller T under strong communication and gradually increase T as communication becomes weaker. Designing adaptive online strategies for selecting T without oracle access is an interesting direction for future work.

Summary of Findings. Across all experiments, we observe a consistent pattern: topology-aware alternating updates provide limited benefit under strong communication, but become increasingly advantageous as communication becomes sparse. Crucially, the optimal switching interval is not fixed, but varies systematically with the underlying communication topology.

As communication becomes weaker, larger switching intervals are preferred, which aligns with our theoretical analysis of topology-induced errors and alternation bias. These results highlight the importance of jointly considering communication topology and switching schedules in decentralized parameter-efficient tuning.

VII. CONCLUSION

In this work, we introduced TAD-LoRA, a topology-aware alternating update framework for decentralized federated fine-tuning. Unlike existing alternating LoRA methods that treat the switching interval as a fixed or monotonic design choice, we identified a previously underexplored trade-off in decentralized settings: overly frequent alternation leads to misalignment between LoRA blocks, while overly infrequent alternation amplifies cross-term noise under stale and sparse communication. We showed that this trade-off induces a non-monotonic dependence on the switching interval T , fundamentally distinguishing decentralized alternating LoRA from its centralized counterpart. We further provided theoretical analysis that characterize how communication topology and sparsity influence the convergence and switching interval selection, revealing that weaker communication favors larger switching intervals. These insights provide useful guidance for the design of practical topology-aware switching strategies in decentralized fine-tuning.

Extensive experiments on GLUE benchmarks validate our analysis. Across a wide range of communication scenarios, TAD-LoRA consistently matches or outperforms decentralized baselines, and outperforms prior alternating methods that are designed for centralized training. Notably, the performance gains become increasingly pronounced as communication becomes sparse, reflecting the fundamental mismatch between centralized alternation strategies and decentralized communication dynamics, and demonstrating that topology-aware coordination yields robust and effective performance in decentralized fine-tuning.

Future Work. Several promising directions remain. First, while this work focuses on topology-aware switching strategies, our theoretical analysis suggests the potential of adaptive

switching policies that adjust T online based on communication conditions or observed training dynamics.

Second, extending TAD-LoRA to larger language models and longer training horizons would further assess its scalability and practical impact. Finally, exploring more structured and realistic communication patterns beyond random and regular topologies remains an important direction for future research.

REFERENCES

- [1] J. Achiam, S. Adler, S. Agarwal, L. Ahmad, I. Akkaya, F. L. Aleman, D. Almeida, J. Altenschmidt, S. Altman, S. Anadkat *et al.*, “Gpt-4 technical report,” *arXiv preprint arXiv:2303.08774*, 2023.
- [2] H. Touvron, T. Lavril, G. Izacard, X. Martinet, M.-A. Lachaux, T. Lacroix, B. Rozière, N. Goyal, E. Hambro, F. Azhar *et al.*, “Llama: Open and efficient foundation language models,” *arXiv preprint arXiv:2302.13971*, 2023.
- [3] A. Zeng, X. Liu, Z. Du, Z. Wang, H. Lai, M. Ding, Z. Yang, Y. Xu, W. Zheng, X. Xia *et al.*, “Glm-130b: An open bilingual pre-trained model,” in *The Eleventh International Conference on Learning Representations*.
- [4] A. Liu, B. Feng, B. Xue, B. Wang, B. Wu, C. Lu, C. Zhao, C. Deng, C. Zhang, C. Ruan *et al.*, “Deepseek-v3 technical report,” *arXiv preprint arXiv:2412.19437*, 2024.
- [5] E. J. Hu, P. Wallis, Z. Allen-Zhu, Y. Li, S. Wang, L. Wang, W. Chen *et al.*, “Lora: Low-rank adaptation of large language models,” in *International Conference on Learning Representations*.
- [6] Z. Wang, Z. Shen, Y. He, G. Sun, H. Wang, L. Lyu, and A. Li, “Flora: Federated fine-tuning large language models with heterogeneous low-rank adaptations,” in *The Thirty-eighth Annual Conference on Neural Information Processing Systems*.
- [7] J. Bai, D. Chen, B. Qian, L. Yao, and Y. Li, “Federated fine-tuning of large language models under heterogeneous tasks and client resources,” in *The Thirty-eighth Annual Conference on Neural Information Processing Systems*, 2024. [Online]. Available: <https://openreview.net/forum?id=gkOzoHBXUw>
- [8] Y. Sun, Z. Li, Y. Li, and B. Ding, “Improving lora in privacy-preserving federated learning,” in *The Twelfth International Conference on Learning Representations*.
- [9] S. Chen, Y. Guo, Y. Ju, H. Dalal, Z. Zhu, and A. Khisti, “Robust federated finetuning of llms via alternating optimization of lora,” *arXiv preprint arXiv:2502.01755*, 2025.
- [10] X. Wang, G. Xiong, H. Cao, J. Li, and Y. Liu, “Decentralized federated learning with model caching on mobile agents,” in *Proceedings of the AAAI Conference on Artificial Intelligence*, vol. 39, no. 20, 2025, pp. 21 296–21 303.
- [11] B. McMahan, E. Moore, D. Ramage, S. Hampson, and B. A. y Arcas, “Communication-efficient learning of deep networks from decentralized data,” in *Artificial intelligence and statistics*. PMLR, 2017, pp. 1273–1282.
- [12] Y. Zhao, M. Li, L. Lai, N. Suda, D. Civin, and V. Chandra, “Federated learning with non-iid data,” *arXiv preprint arXiv:1806.00582*, 2018.
- [13] T. Li, A. K. Sahu, A. Talwalkar, and V. Smith, “Federated learning: Challenges, methods, and future directions,” *IEEE signal processing magazine*, vol. 37, no. 3, pp. 50–60, 2020.
- [14] P. Kairouz, H. B. McMahan, B. Avent, A. Bellet, M. Bennis, A. N. Bhagoji, K. Bonawitz, Z. Charles, G. Cormode, R. Cummings *et al.*, “Advances and open problems in federated learning,” *Foundations and trends® in machine learning*, vol. 14, no. 1–2, pp. 1–210, 2021.
- [15] F. Sattler, S. Wiedemann, K.-R. Müller, and W. Samek, “Robust and communication-efficient federated learning from non-iid data,” *IEEE transactions on neural networks and learning systems*, vol. 31, no. 9, pp. 3400–3413, 2019.
- [16] A. F. Aji and K. Heafield, “Sparse communication for distributed gradient descent,” in *Proceedings of the 2017 Conference on Empirical Methods in Natural Language Processing*, 2017, pp. 440–445.
- [17] A. Fallah, A. Mokhtari, and A. Ozdaglar, “Personalized federated learning with theoretical guarantees: A model-agnostic meta-learning approach,” *Advances in neural information processing systems*, vol. 33, pp. 3557–3568, 2020.
- [18] X. Lian, C. Zhang, H. Zhang, C.-J. Hsieh, W. Zhang, and J. Liu, “Can decentralized algorithms outperform centralized algorithms? a case study for decentralized parallel stochastic gradient descent,” *Advances in neural information processing systems*, vol. 30, 2017.
- [19] A. Lalitha, O. C. Kılınç, T. Javidi, and F. Koushanfar, “Peer-to-peer federated learning on graphs,” *arXiv preprint arXiv:1901.11173*, 2019.
- [20] C. Xie, S. Koyejo, and I. Gupta, “Asynchronous federated optimization,” *arXiv preprint arXiv:1903.03934*, 2019.
- [21] S. Babakniya, A. R. Elkordy, Y. H. Ezzeldin, Q. Liu, K.-B. Song, M. EL-Khamy, and S. Avestimehr, “Slora: Federated parameter efficient fine-tuning of language models,” in *International Workshop on Federated Learning in the Age of Foundation Models in Conjunction with NeurIPS 2023*.
- [22] P. Guo, S. Zeng, Y. Wang, H. Fan, F. Wang, and L. Qu, “Selective aggregation for low-rank adaptation in federated learning,” in *The Thirteenth International Conference on Learning Representations*, 2025. [Online]. Available: <https://openreview.net/forum?id=iX3uESGdsO>
- [23] L. Yi, H. Yu, G. Wang, X. Liu, and X. Li, “pfedlora: Model-heterogeneous personalized federated learning with lora tuning,” 2024. [Online]. Available: <https://arxiv.org/abs/2310.13283>
- [24] X. Yu, Y. Wang, J. Chen, and L. Xue, “Altllora: Towards better gradient approximation in low-rank adaptation with alternating projections,” *arXiv preprint arXiv:2505.12455*, 2025.
- [25] P. Erdős and A. R&wi, “On random graphs i,” *Publ. math. debrecen*, vol. 6, no. 290-297, p. 18, 1959.

APPENDIX A FULL THEORETICAL ANALYSIS

This appendix provides the complete convergence analysis supporting Section V. While the main text highlights the key trade-off, here we explicitly detail the role of the LoRA product structure, the cross-term induced by decentralized aggregation, and the blockwise optimization bias caused by alternating updates with period T .

Roadmap. Our analysis proceeds through the following key components:

- 1) **Per-block consensus:** Establishing that frozen blocks contract purely via gossip, while updated blocks incur bounded error.
- 2) **Decomposition:** Splitting the averaged LoRA update into a "centralized-equivalent" factor term and a topology-dependent cross term.
- 3) **Cross-term decay:** Proving that the accumulated topology error decreases as $O(1/T)$ within each alternating cycle.
- 4) **Representation bias:** Quantifying the drift caused by optimizing against stale parameters, which increases with T .
- 5) **Main Convergence:** Combining these effects to derive the stationarity bound and the topology-dependent optimal switching period T^* .

A. Notation and Preliminaries

Norm convention. Unless otherwise specified, $\|\cdot\|$ denotes the Euclidean norm for vectors and the Frobenius norm for matrices.

LoRA Formulation. Each client i holds LoRA parameters (A_i^t, B_i^t) and the local model is $\theta_i^t = \theta_0 + B_i^t A_i^t$. We denote global averages as:

$$\bar{A}^t = \frac{1}{m} \sum_{i=1}^m A_i^t, \quad \bar{B}^t = \frac{1}{m} \sum_{i=1}^m B_i^t, \quad \bar{\theta}^t = \frac{1}{m} \sum_{i=1}^m \theta_i^t.$$

Communication Topology. Let W_t be the random doubly-stochastic mixing matrix. We assume the network satisfies the spectral gap property:

$$\mathbb{E} \left\| W_t - \frac{1}{m} \mathbf{1} \mathbf{1}^\top \right\|_2^2 \leq \rho^2, \quad 0 < \rho < 1.$$

Reference Optimum ($T = 1$). To quantify the bias of coarse-grained switching ($T > 1$), we define the *reference optimum* θ_1^* as the optimal solution attained by an ideal centralized alternating LoRA method with $T = 1$ (switching every step). Let $F_1^* := F(\theta_1^*)$. This serves as the baseline for our suboptimality analysis.

B. Assumptions

We first state standard regularity assumptions commonly used in decentralized stochastic optimization.

Assumption A.1 (Regularity Conditions). The following conditions hold:

- **L-Smoothness:** Each local objective f_i is L -smooth.
- **Stochastic Gradients:** Local stochastic gradients are unbiased and have bounded second moments (variance σ^2).
- **Mixing Contraction:** The mixing matrices W_t satisfy the mean-square contraction property defined in Section A-A.

In addition to standard regularity, our analysis requires two structural assumptions specific to the alternating LoRA landscape, as introduced in the main text.

Assumption A.2 (Local PL on the LoRA subspace). (Restatement of Assumption V.1). There exists $\mu > 0$ such that for all θ in a neighborhood of θ_1^* ,

$$F(\theta) - F_1^* \leq \frac{1}{2\mu} \|\nabla F(\theta)\|^2.$$

Assumption A.3 (Alternating-induced factorization bias). (Restatement of Assumption V.2). Let F_T^* denote the optimal value achievable with switching interval T . There exists $C_3 > 0$ such that for sufficiently small stepsize η :

$$\phi(T) := F_T^* - F_1^* \leq C_3 T \eta^2.$$

C. Per-Block Consensus Under Alternating Updates

We analyze the consensus error $\Delta_A^t := A^t - \bar{A}^t$.

Lemma A.4 (Per-block consensus). *Under the standing assumptions (spectral gap ρ and bounded gradient variance σ^2), for stepsize η :*

- **Updated Block:** $\mathbb{E} \|\Delta_A^{t+1}\|^2 \leq \frac{1+\rho^2}{2} \mathbb{E} \|\Delta_A^t\|^2 + C_{\text{blk}} \eta^2$.
- **Frozen Block:** $\mathbb{E} \|\Delta_A^{t+1}\|^2 \leq \rho^2 \mathbb{E} \|\Delta_A^t\|^2$.

Proof. **Case 1: Frozen Block.** The update is purely communicative: $A_i^{t+1} = \sum_j W_{ij} A_j^t$. In matrix form, this is $\Delta_A^{t+1} = (W_t - \frac{1}{m} \mathbf{1} \mathbf{1}^\top) \Delta_A^t$. Taking the norm and applying the spectral gap definition directly yields $\mathbb{E} \|\Delta_A^{t+1}\|^2 \leq \rho^2 \mathbb{E} \|\Delta_A^t\|^2$. **Case 2: Updated Block.** The update includes a gradient term: $A_i^{t+1} = \sum_j W_{ij} A_j^t - \eta g_i^t$. The error decomposes into a mixing part and a noise part: $\Delta_A^{t+1} = (W_t - \frac{1}{m} \mathbf{1} \mathbf{1}^\top) \Delta_A^t - \eta (I - \frac{1}{m} \mathbf{1} \mathbf{1}^\top) g^t$. Using the inequality $\|X + Y\|^2 \leq (1 + \gamma) \|X\|^2 + (1 + \frac{1}{\gamma}) \|Y\|^2$ to separate the terms, and bounding the gradient variance, we obtain the stated result. \square

Steady-state disagreement. From Lemma A.4, $u_{t+1} \leq \rho^2 u_t + C_{\text{blk}} \eta^2 G^2$ with $u_t := \mathbb{E} \|\Delta_B^t\|^2$, hence $u_t \leq \rho^{2t} u_0 + C_{\text{blk}} \eta^2 G^2 \sum_{s=0}^{t-1} \rho^{2s} \leq \rho^{2t} u_0 + \frac{C_{\text{blk}} \eta^2 G^2}{1-\rho^2} = O(\eta^2/(1-\rho))$ after a transient, and similarly for Δ_A^t .

D. Cross-Term Decomposition

We decompose the global update to isolate topology-induced errors. The averaged LoRA update matrix is $\bar{W}^t := \frac{1}{m} \sum_{i=1}^m B_i^t A_i^t$. Adding and subtracting the product of averages $\bar{B}^t \bar{A}^t$ yields:

$$\bar{W}^t = \bar{B}^t \bar{A}^t + C^t, \quad \text{where } C^t := \frac{1}{m} \sum_{i=1}^m (B_i^t - \bar{B}^t)(A_i^t - \bar{A}^t).$$

By Cauchy–Schwarz, the norm of this cross term is bounded by the product of disagreements:

$$\|C^t\|_F \leq \sqrt{\frac{1}{m} \sum \|B_i^t - \bar{B}^t\|^2} \cdot \sqrt{\frac{1}{m} \sum \|A_i^t - \bar{A}^t\|^2} = \|\Delta_A^t\| \|\Delta_B^t\|.$$

Effect on Optimization. Assuming the objective function is G -Lipschitz (bounded gradients), the perturbation in the objective value caused by C^t is bounded by:

$$|F(\bar{\theta}^t) - F(\theta_0 + \bar{B}^t \bar{A}^t)| \leq G \|C^t\|_F \leq G \|\Delta_A^t\| \|\Delta_B^t\|.$$

This explicitly connects the topology error to the optimization objective: minimizing blockwise disagreement minimizes the deviation from the centralized trajectory.

E. Cross-Term Decay Within an Alternating Cycle

Proposition A.5 (Cycle-averaged cross-term decay). *For any alternating cycle of length T ,*

$$\frac{1}{T} \sum_{\tau=0}^{T-1} \mathbb{E} \|C^{t+\tau}\|_F \leq \frac{C_{\text{cr}} \eta^2}{T(1-\rho)}$$

for a constant $C_{\text{cr}} > 0$ independent of T and ρ .

Proof. Recall $\|C^t\|_F \leq \|\Delta_A^t\| \|\Delta_B^t\|$. Consider a phase of length T in which block A is frozen and block B is updated. By Lemma A.4, for $\tau = 0, \dots, T-1$,

$$\mathbb{E} \|\Delta_A^{t+\tau}\|^2 \leq \rho^{2\tau} \mathbb{E} \|\Delta_A^t\|^2.$$

Meanwhile, during the update phase, the disagreement of the updated block reaches a steady-state level $\mathbb{E} \|\Delta_B^{t+\tau}\|^2 \leq C \eta^2 / (1-\rho)$. Using Cauchy–Schwarz and Jensen,

$$\mathbb{E} \|C^{t+\tau}\|_F \leq \sqrt{\mathbb{E} \|\Delta_A^{t+\tau}\|^2} \sqrt{\mathbb{E} \|\Delta_B^{t+\tau}\|^2} \leq \rho^\tau \sqrt{\mathbb{E} \|\Delta_A^t\|^2} \cdot \sqrt{\frac{C \eta^2}{1-\rho}}.$$

Averaging over τ yields a geometric series:

$$\frac{1}{T} \sum_{\tau=0}^{T-1} \mathbb{E} \|C^{t+\tau}\|_F \leq \frac{1}{T} \left(\sum_{\tau=0}^{T-1} \rho^\tau \right) \sqrt{\mathbb{E} \|\Delta_A^t\|^2} \cdot \sqrt{\frac{C \eta^2}{1-\rho}}.$$

After the transient, Lemma A.4 implies $\mathbb{E} \|\Delta_A^t\|^2 \leq C' \eta^2 / (1-\rho)$. Substituting and using $\sum_{\tau=0}^{T-1} \rho^\tau \leq \frac{1}{1-\rho}$ gives

$$\frac{1}{T} \sum_{\tau=0}^{T-1} \mathbb{E} \|C^{t+\tau}\|_F \leq \frac{C_{\text{cr}} \eta^2}{T(1-\rho)},$$

which proves the claim. This shows that the cycle-averaged cross term decreases as $O(1/T)$.

F. One-step Descent of the Averaged Model

Lemma A.6 (One-step descent of the averaged model). *Suppose F is L -smooth and the averaged iterate satisfies $\bar{\theta}^{t+1} = \bar{\theta}^t - \eta g^t$, where $g^t = \frac{1}{m} \sum_i g_i^t$. Then for sufficiently small η ,*

$$\mathbb{E}[F(\bar{\theta}^{t+1})] \leq \mathbb{E}[F(\bar{\theta}^t)] - \eta \mathbb{E}\|\nabla F(\bar{\theta}^t)\|^2 + C\eta^2(1 + \mathbb{E}\|\Delta_A^t\|^2 + \mathbb{E}\|\Delta_B^t\|^2 + \mathbb{E}\|C^t\|_F).$$

Proof. By L -smoothness (descent lemma),

$$F(\bar{\theta}^{t+1}) \leq F(\bar{\theta}^t) - \eta \langle \nabla F(\bar{\theta}^t), g^t \rangle + \frac{L\eta^2}{2} \|g^t\|^2.$$

Take conditional expectation w.r.t. the randomness at time t and use $\mathbb{E}[g^t | \mathcal{F}_t] = \frac{1}{m} \sum_i \nabla f_i(\theta_i^t)$.

Gradient decomposition. Write

$$g^t = \nabla F(\bar{\theta}^t) + e_{\text{cons}}^t + e_{\text{noise}}^t,$$

where

$$e_{\text{cons}}^t := \frac{1}{m} \sum_{i=1}^m (\nabla f_i(\theta_i^t) - \nabla f_i(\bar{\theta}^t)), \quad e_{\text{noise}}^t := \frac{1}{m} \sum_{i=1}^m (g_i^t - \nabla f_i(\theta_i^t)).$$

By unbiased stochastic gradients and bounded variance,

$$\mathbb{E}[e_{\text{noise}}^t | \mathcal{F}_t] = 0, \quad \mathbb{E}[\|e_{\text{noise}}^t\|^2 | \mathcal{F}_t] \leq \frac{\sigma^2}{m} \leq C.$$

Bounding the consensus/heterogeneity term via LoRA factor disagreements and the cross term. Using L -smoothness of each f_i ,

$$\|e_{\text{cons}}^t\| \leq \frac{1}{m} \sum_{i=1}^m \|\nabla f_i(\theta_i^t) - \nabla f_i(\bar{\theta}^t)\| \leq \frac{L}{m} \sum_{i=1}^m \|\theta_i^t - \bar{\theta}^t\|.$$

Now decompose the model deviation using the LoRA product structure:

$$\theta_i^t - \bar{\theta}^t = (\theta_0 + B_i^t A_i^t) - (\theta_0 + \bar{B}^t \bar{A}^t + C^t) = \underbrace{(B_i^t A_i^t - \bar{B}^t \bar{A}^t)}_{\text{factor disagreement}} - \underbrace{C^t}_{\text{cross term}}.$$

Hence,

$$\|\theta_i^t - \bar{\theta}^t\| \leq \|B_i^t A_i^t - \bar{B}^t \bar{A}^t\| + \|C^t\|_F.$$

Applying $\|XY\|_F \leq \|X\|_F \|Y\|_2$ and standard bilinear expansion yields (for bounded factor norms, absorbed into the constant)

$$\frac{1}{m} \sum_{i=1}^m \|B_i^t A_i^t - \bar{B}^t \bar{A}^t\|^2 \leq C(\|\Delta_A^t\|^2 + \|\Delta_B^t\|^2).$$

Combining the above bounds and Jensen's inequality gives

$$\mathbb{E}\|e_{\text{cons}}^t\|^2 \leq C(\mathbb{E}\|\Delta_A^t\|^2 + \mathbb{E}\|\Delta_B^t\|^2 + \mathbb{E}\|C^t\|_F),$$

where we used $\|C^t\|_F^2 \leq \|C^t\|_F$ after absorbing constants (or equivalently replace $\mathbb{E}\|C^t\|_F$ by $\mathbb{E}\|C^t\|_F^2$ if you prefer a squared term).

Putting pieces together. Plugging $g^t = \nabla F(\bar{\theta}^t) + e_{\text{cons}}^t + e_{\text{noise}}^t$ into the descent lemma and expanding,

$$-\eta \langle \nabla F(\bar{\theta}^t), g^t \rangle = -\eta \|\nabla F(\bar{\theta}^t)\|^2 - \eta \langle \nabla F(\bar{\theta}^t), e_{\text{cons}}^t \rangle - \eta \langle \nabla F(\bar{\theta}^t), e_{\text{noise}}^t \rangle.$$

Apply Young's inequality $\langle a, b \rangle \leq \frac{1}{4}\|a\|^2 + \|b\|^2$ to the two inner products to obtain

$$-\eta \langle \nabla F(\bar{\theta}^t), e_{\text{cons}}^t \rangle \leq \frac{\eta}{4} \|\nabla F(\bar{\theta}^t)\|^2 + \eta \|e_{\text{cons}}^t\|^2, \quad -\eta \langle \nabla F(\bar{\theta}^t), e_{\text{noise}}^t \rangle \leq \frac{\eta}{4} \|\nabla F(\bar{\theta}^t)\|^2 + \eta \|e_{\text{noise}}^t\|^2.$$

Similarly, $\|g^t\|^2 \leq C(\|\nabla F(\bar{\theta}^t)\|^2 + \|e_{\text{cons}}^t\|^2 + \|e_{\text{noise}}^t\|^2)$. Taking expectation and choosing η sufficiently small so that the $\eta^2 \mathbb{E}\|\nabla F(\bar{\theta}^t)\|^2$ term can be absorbed into the main descent term yields

$$\mathbb{E}[F(\bar{\theta}^{t+1})] \leq \mathbb{E}[F(\bar{\theta}^t)] - \eta \mathbb{E}\|\nabla F(\bar{\theta}^t)\|^2 + C\eta^2(1 + \mathbb{E}\|\Delta_A^t\|^2 + \mathbb{E}\|\Delta_B^t\|^2 + \mathbb{E}\|C^t\|_F),$$

which proves the claim. \square

G. Topology-Induced Stationarity Bound

We now combine the one-step descent result in Lemma A.6 with steady-state block disagreements and the cycle-averaged cross-term decay (Proposition A.5) to derive a stationarity bound.

Theorem A.7 (Stationarity under alternating LoRA).

$$\frac{1}{R} \sum_{t=0}^{R-1} \mathbb{E} \|\nabla F(\bar{\theta}^t)\|^2 \leq \frac{C_0}{\eta R} + C_1 \eta + \frac{C_2 \eta^2}{T(1-\rho)} + O(\eta^2).$$

The last term $\frac{C_2 \eta^2}{T(1-\rho)}$ corresponds exactly to the cross-term decay in Section A-E.

Representation bias induced by coarse switching. We now interpret the term $\phi(T)$ introduced in Assumption A.3. This assumption captures the inherent cost of freezing one LoRA factor for T consecutive updates. When one block is optimized against a stale counterpart, a deterministic approximation error is introduced. Under standard smoothness, this mismatch incurs a per-step error of order $O(\eta^2)$, which accumulates linearly over the freezing horizon T . As a result,

$$\phi(T) = F_T^* - F_1^* \leq C_3 T \eta^2.$$

This term reflects a representation-level bias that is independent of the communication topology, and it increases monotonically with the switching interval T .

PL condition (restatement of Assumption V.1). We assume the local PL condition stated in Assumption V.1.

Remark. The PL condition is imposed only locally around the reference optimum θ_1^* and is used to relate gradient stationarity to function-value suboptimality. It does not require the algorithm to operate with switching interval $T = 1$, nor does it restrict the optimization trajectory to follow the $T = 1$ alternating scheme.

H. Suboptimality relative to the reference optimum

Theorem A.8 (Function-value gap).

$$\mathbb{E}[F(\hat{\theta}_R) - F_1^*] \leq \frac{1}{2\mu} \left(\frac{C_0}{\eta R} + C_1 \eta + \frac{C_2}{T(1-\rho)} \right) + \phi(T).$$

The term $C_2/[T(1-\rho)]$ comes from cross-term topology effects, while $\phi(T)$ captures block-coordinate bias from Assumption V.2. $F_1^* := F(\theta_1^*)$ denotes the objective value at the reference optimum defined in Section A-A. Let $\hat{\theta}_R$ be chosen uniformly from $\{\hat{\theta}^0, \dots, \hat{\theta}^{R-1}\}$.

I. Topology-Dependent Optimal Switching Period

Define

$$\Psi(T; \rho) := \frac{C_2}{T(1-\rho)} + \phi(T).$$

Corollary A.9 (Optimal switching interval).

$$T^*(\rho) \in \arg \min_{T \geq 1} \Psi(T; \rho).$$

Under Assumption V.2,

$$\Psi(T; \rho) \leq \frac{C_2}{T(1-\rho)} + C_3 T \eta^2,$$

whose minimizer satisfies

$$T^*(\rho) \in \Theta\left(\frac{1}{\sqrt{1-\rho}}\right).$$

Interpretation.

Small T : cross-term dominates $\frac{1}{T(1-\rho)}$.	Large T : block-coordinate bias dominates $\phi(T) \sim T \eta^2$.
--	---

The optimal T^* balances the two sources of error.

J. Edge-activation gossip and spectral gap scaling

Lemma A.10 (Edge-activation gossip implies a spectral gap scaling). *Consider a fixed connected undirected graph $G = (V, E)$ with $m := |V|$ nodes and (combinatorial) Laplacian L . At iteration t , each edge $e = (i, j) \in E$ is activated independently with probability $p \in (0, 1]$. For every activated edge, a pairwise averaging update is performed between its incident nodes:*

$$x_i \leftarrow \frac{1}{2}(x_i + x_j), \quad x_j \leftarrow \frac{1}{2}(x_i + x_j),$$

and if a node participates in multiple activated edges, the corresponding pairwise updates are applied in a uniformly random order within the iteration. Let the resulting one-iteration mixing matrix be W_t (so $x^{t+1} = W_t x^t$). Then W_t is doubly-stochastic and satisfies the mean-square contraction assumption

$$\mathbb{E} \left\| W_t - \frac{1}{m} \mathbf{1} \mathbf{1}^\top \right\|_2^2 \leq \rho^2$$

for some $\rho \in (0, 1)$. Moreover, there exists a constant $c_{\text{mix}} > 0$ (depending only on the averaging rule and the maximum degree of G , but independent of p, T, R) such that the effective spectral gap obeys

$$1 - \rho \geq c_{\text{mix}} p \lambda_2(L).$$

Proof sketch. Let $J := \frac{1}{m} \mathbf{1} \mathbf{1}^\top$ and define the disagreement vector $y := (I - J)x$ so that $y \perp \mathbf{1}$. It suffices to control the contraction of $\|y\|^2$ in one iteration. For a single activated edge $e = (i, j)$, the pairwise averaging matrix can be written as

$$W_e = I - \frac{1}{2} L_e,$$

where L_e is the rank-1 Laplacian associated with edge e . When multiple edges are activated, the within-iteration random-order update yields

$$W_t = \prod_{e \in E_t} W_e,$$

where $E_t \subseteq E$ is the random set of activated edges. Using the standard (Lie/Trotter-type) first-order approximation for products of near-identity averaging operators, one obtains the Laplacian-averaging abstraction

$$W_t \approx I - \alpha L_t, \quad L_t := \sum_{e \in E_t} L_e,$$

for some constant step size $\alpha \in (0, 1]$ determined by the averaging rule. Since each edge is activated independently with probability p ,

$$\mathbb{E}[L_t] = p \sum_{e \in E} L_e = pL, \quad \Rightarrow \quad \mathbb{E}[W_t] \approx I - \alpha pL.$$

Because $L\mathbf{1} = 0$ and L is symmetric PSD with eigenvalues $0 = \lambda_1(L) < \lambda_2(L) \leq \dots \leq \lambda_m(L)$, we have

$$\lambda_2(\mathbb{E}[W_t]) \approx 1 - \alpha p \lambda_2(L),$$

so the spectral gap scales linearly in $p \lambda_2(L)$. Finally, in symmetric doubly-stochastic settings, the mean-square contraction $\mathbb{E} \|W_t - J\|_2^2$ can be upper bounded (up to constants) by the second eigenvalue of $\mathbb{E}[W_t^\top W_t]$, which inherits the same linear scaling for sufficiently small α . Absorbing approximation and higher-order terms into c_{mix} yields $1 - \rho \geq c_{\text{mix}} p \lambda_2(L)$. \square

Corollary A.11 (Optimal switching interval under independent edge activation). *Consider the independent edge activation model on a fixed underlying graph $G = (V, E)$: at each iteration, every edge is activated independently with probability $p \in (0, 1]$, and activated edges perform pairwise averaging updates (with a random order when a node participates in multiple activated edges). Let L be the (combinatorial) Laplacian of G and $\lambda_2(L)$ be its algebraic connectivity.*

Assume the induced mixing matrix W_t satisfies the mean-square contraction assumption

$$\mathbb{E} \left\| W_t - \frac{1}{m} \mathbf{1} \mathbf{1}^\top \right\|_2^2 \leq \rho^2,$$

and moreover the effective spectral gap scales as

$$1 - \rho \geq c_{\text{mix}} p \lambda_2(L),$$

for some constant $c_{\text{mix}} > 0$ determined by the averaging rule (e.g., the effective step size in the Laplacian-averaging abstraction) and independent of p, T, R .

Then the dominant T -dependent error term in Theorem A-H can be written as

$$\Psi(T; p, L) := \frac{C_2}{T(1 - \rho)} + \phi(T) \leq \frac{\tilde{C}_2}{T p \lambda_2(L)} + \phi(T),$$

where $\tilde{C}_2 := C_2/c_{\text{mix}}$.

Consequently, an optimal switching interval satisfies

$$T^*(p, L) \in \arg \min_{T \geq 1} \left\{ \frac{\tilde{C}_2}{T p \lambda_2(L)} + \phi(T) \right\}.$$

If in addition the alternating-induced bias obeys $\phi(T) \leq C_3 T \eta^2$, then balancing the two dominant terms yields

$$T^*(p, L) \in \Theta \left(\frac{1}{\sqrt{p \lambda_2(L)}} \right).$$

In particular, better connectivity (larger $\lambda_2(L)$) and more reliable communication (larger p) both lead to smaller optimal switching intervals.

K. Scope of the analysis.

All local regularity conditions (e.g., PL and smoothness on the LoRA subspace) are imposed with respect to the reference optimum θ_1^* and are used solely to convert stationarity guarantees into function-value bounds. They do not impose any restriction on the switching interval T used by the decentralized algorithm.

APPENDIX B ADDITIONAL EXPERIMENTAL RESULTS

A. Additional Communication Probabilities.

Table II reports additional results under communication probabilities $p \in \{0.2, 0.1, 0.05, 0.01\}$, which are not included in the main results due to space constraints. The same evaluation protocol as in the main paper is used, reporting test accuracy as mean \pm variance over 3 random seeds.

These additional results provide a more complete picture of how different methods behave across a wide range of communication regimes. As the communication probability decreases, performance degradation is observed for all methods, which is expected due to reduced model exchanges. Nevertheless, TAD-LoRA consistently achieves the strongest performance under low communication probabilities, not only in terms of the average across datasets, but also on individual tasks.

Best and second-best results for each dataset under the same communication probability are highlighted to emphasize per-dataset robustness. This demonstrates that the gains of TAD-LoRA under sparse communication are consistent across heterogeneous tasks, rather than being driven by a single dataset.

B. Weak-Regime Performance Summary

We define the weak communication regime as $p \leq 0.05$. Table III reports the average performance obtained by uniformly averaging the per- p average accuracy across datasets. This summary complements the main results by highlighting the robust advantage of TAD-LoRA under communication-constrained settings.

C. Illustrative non-monotonic behavior.

Figure 5 provides a representative example of the non-monotonic dependence on the switching interval predicted by our theory. In practice, the idealized U-shaped behavior is obscured by training noise, discrete alternation schedules, and finite training budgets, resulting in a range of effective switching intervals rather than a single sharp optimum. This observation is consistent with the aggregate trends and heatmap visualizations reported in the main paper.

D. Additional Network Topologies

1) *Ring Topology*: Beyond the representative random (Erdős–Rényi) communication topology considered in the main results, we further evaluate TAD-LoRA under a ring topology, which represents a highly structured network with limited connectivity and slow information mixing. This setting serves as an extreme stress test rather than a typical deployment scenario.

As shown in Table V, all methods experience reduced performance compared to random topologies, which is expected due to the restricted information propagation in a ring. Nevertheless, TAD-LoRA remains competitive with baseline methods and achieves comparable average accuracy with stable variance. In particular, TAD-LoRA attains the best performance on the more challenging MNLI task, while consistently outperforming other alternating baselines.

Overall, these results indicate that while the advantage of topology-aware coordination is diminished when the network structure itself becomes the dominant bottleneck, TAD-LoRA does not introduce additional instability or degradation under extremely constrained topologies.

TABLE II: Full results under communication probabilities. Test accuracy is reported as mean \pm variance over 3 random seeds. Best and second-best results for each dataset under the same p are highlighted in bold and underline, respectively.

p	Method	SST-2	QQP	QNLI	MNLI	Avg.
0.5	LoRA	0.9468 \pm 0.0019	0.8347 \pm 0.0085	0.9067 \pm 0.0043	0.8132 \pm 0.0194	0.8754
	FFA-LoRA	0.9436 \pm 0.0032	0.8051 \pm 0.0061	0.8911 \pm 0.0036	0.7313 \pm 0.0333	0.8428
	RoLoRA	<u>0.9462</u> \pm 0.0023	0.8216 \pm 0.0108	<u>0.9021</u> \pm 0.0031	0.8115 \pm 0.0088	0.8703
	TAD-LoRA (Ours)	0.9448 \pm 0.0007	<u>0.8328</u> \pm 0.0072	0.9003 \pm 0.0048	0.8145 \pm 0.0066	<u>0.8731</u>
0.2	LoRA	<u>0.9451</u> \pm 0.0049	0.8202 \pm 0.0059	<u>0.8950</u> \pm 0.0117	<u>0.7933</u> \pm 0.0098	<u>0.8634</u>
	FFA-LoRA	0.9365 \pm 0.0025	0.7996 \pm 0.0047	0.8859 \pm 0.0032	0.7300 \pm 0.0285	<u>0.8380</u>
	RoLoRA	0.9407 \pm 0.0017	<u>0.8119</u> \pm 0.0142	0.8826 \pm 0.0065	0.7693 \pm 0.0140	0.8511
	TAD-LoRA (Ours)	0.9453 \pm 0.0038	0.8254 \pm 0.0019	0.8953 \pm 0.0030	0.7974 \pm 0.0107	0.8659
0.1	LoRA	<u>0.9370</u> \pm 0.0058	0.8098 \pm 0.0076	<u>0.8779</u> \pm 0.0159	<u>0.7253</u> \pm 0.0440	<u>0.8375</u>
	FFA-LoRA	0.9313 \pm 0.0046	0.7915 \pm 0.0086	0.8710 \pm 0.0048	0.7086 \pm 0.0242	0.8256
	RoLoRA	0.9325 \pm 0.0048	0.7890 \pm 0.0027	0.8711 \pm 0.0045	0.7113 \pm 0.0133	0.8260
	TAD-LoRA (Ours)	0.9401 \pm 0.0019	<u>0.8050</u> \pm 0.0073	0.8815 \pm 0.0145	0.7405 \pm 0.0376	0.8418
0.05	LoRA	<u>0.9330</u> \pm 0.0030	<u>0.7923</u> \pm 0.0133	<u>0.8764</u> \pm 0.0071	<u>0.7102</u> \pm 0.0088	<u>0.8280</u>
	FFA-LoRA	0.9263 \pm 0.0043	0.7814 \pm 0.0145	0.8659 \pm 0.0147	0.6699 \pm 0.0079	<u>0.8109</u>
	RoLoRA	0.9238 \pm 0.0036	0.7851 \pm 0.0089	0.8424 \pm 0.0129	0.6818 \pm 0.0130	0.8083
	TAD-LoRA (Ours)	0.9328 \pm 0.0033	0.7965 \pm 0.0118	0.8743 \pm 0.0130	0.7333 \pm 0.0126	0.8342
0.02	LoRA	0.8668 \pm 0.0811	<u>0.7702</u> \pm 0.0066	0.8416 \pm 0.0031	0.6407 \pm 0.0118	0.7798
	FFA-LoRA	<u>0.9186</u> \pm 0.0038	0.7627 \pm 0.0121	0.8264 \pm 0.0178	0.6191 \pm 0.0358	<u>0.7817</u>
	RoLoRA	0.9147 \pm 0.0022	0.7582 \pm 0.0116	0.8160 \pm 0.0045	0.5980 \pm 0.0291	<u>0.7717</u>
	TAD-LoRA (ours)	0.9263 \pm 0.0019	0.7783 \pm 0.0036	0.8480 \pm 0.0063	0.6604 \pm 0.0408	0.8032
0.01	LoRA	<u>0.9133</u> \pm 0.0044	0.7503 \pm 0.0081	<u>0.8231</u> \pm 0.0123	<u>0.5862</u> \pm 0.0396	<u>0.7682</u>
	FFA-LoRA	0.9123 \pm 0.0040	<u>0.7555</u> \pm 0.0132	0.8178 \pm 0.0080	0.5759 \pm 0.0242	0.7654
	RoLoRA	0.9120 \pm 0.0014	0.7420 \pm 0.0209	0.7974 \pm 0.0143	0.5153 \pm 0.0110	0.7417
	TAD-LoRA (Ours)	0.9190 \pm 0.0024	0.7605 \pm 0.0139	0.8218 \pm 0.0087	0.6092 \pm 0.0178	0.7776

TABLE III: Average performance in the weak communication regime ($p \leq 0.05$).

Method	Weak-Regime Avg. Accuracy
LoRA	0.7920
FFA-LoRA	0.7860
RoLoRA	0.7739
TAD-LoRA (Ours)	0.8050

TABLE IV: Empirically selected optimal switching interval $\hat{T}^*(p)$ under different communication probabilities p . The candidate set is consistent with experimental setting.

p	SST-2	QQP	QNLI	MNLI	Avg.	Median
0.5	1	1	1	3	1.50	1
0.2	1	5	1	5	3.00	3
0.1	5	3	3	3	3.50	3
0.05	5	5	15	5	7.50	5
0.02	3	1	15	15	8.50	9
0.01	10	5	3	3	5.25	4

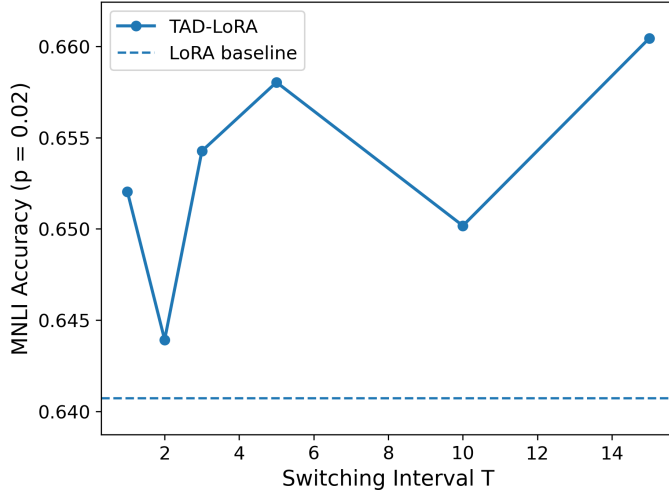


Fig. 5: Illustrative example of the non-monotonic dependence on the switching interval T on MNLI under a weak communication regime ($p = 0.02$). The y-axis reports the accuracy gain of TAD-LoRA over the LoRA baseline. Due to discrete scheduling and training noise, the U-shaped behavior predicted by theory manifests as a noisy and flattened trend rather than a sharp optimum.

TABLE V: Results under a ring communication topology. Test accuracy is reported as mean \pm variance over 3 random seeds. The ring topology represents a structured network with slow information mixing and serves as a stress test for topology-aware methods.

Method	SST-2	QQP	QNLI	MNLI	Avg.
LoRA	0.9464 ± 0.0016	0.8308 ± 0.0057	0.9015 ± 0.0048	0.8185 ± 0.0018	0.8743
FFA-LoRA	0.9392 ± 0.0026	0.8044 ± 0.0096	0.8977 ± 0.0074	0.7728 ± 0.0150	0.8535
RoLoRA	0.9419 ± 0.0002	0.8246 ± 0.0024	0.8957 ± 0.0064	0.7997 ± 0.0112	0.8655
TAD-LoRA	0.9438 ± 0.0012	0.8290 ± 0.0046	0.9010 ± 0.0020	0.8208 ± 0.0046	0.8736